UNIVERSITY
OF TRENTO

DIPARTIMENTO DI INGEGNERIA E SCIENZA DELL'INFORMAZIONE

38123 Povo – Trento (Italy), Via Sommarive 14
http://www.disi.unitn.it

TIME MODULATED PLANAR ARRAYS ANALYSIS AND OPTIMIZATION OF THE SIDEBAND RADIATIONS

L. Poli, P. Rocca, L. Manica, and A. Massa

January 2011

Technical Report # DISI-11-084

Time Modulated Planar Arrays - Analysis and Optimization of the Sideband Radiations

L. Poli, P. Rocca, *Student Member, IEEE,* L. Manica, and A. Massa, *Member, IEEE*

ELEDIA Research Group

Department of Information Engineering and Computer Science,

University of Trento, Via Sommarive 14, 38050 Trento - Italy

Tel. +39 0461 882057, Fax +39 0461 882093

E-mail: *andrea.massa@ing.unitn.it*,

{*lorenzo.poli, paolo.rocca, luca.manica*}*@disi.unitn.it*

Web-site: *http://www.eledia.ing.unitn.it*

Time Modulated Planar Arrays - Analysis and Optimization of the Sideband Radiations

L. Poli, P. Rocca, L. Manica, and A. Massa

Abstract

In this paper, the minimization of the power losses due to undesired sideband radiations in time-modulated planar arrays is dealt with. A closed-form expression for evaluating the total power wasted in the sideband radiations is obtained and exploited to design a new procedure based on a Particle Swarm Optimizer for the synthesis of the pulse sequences devoted to control the array time-modulation. A set of representative results is reported and analyzed to assess the effectiveness of the proposed approach.

Key words: Planar Arrays, Time-Modulated Arrays, Pattern Synthesis.

1 Introduction

After the work by Shanks and Bickmore [1] proposing the time domain as an additional degree of freedom for the control of the radiation characteristics of an antenna system and the first prototype of a time-modulated array for the generation of ultra-low sidelobe patterns in [2], the synthesis of time-modulated (TM) arrays has received a renewed interest in recent years. Different numerical approaches dealing with both linear arrays [3]-[8] and planar arrangements [9]-[12] have been proposed. Time modulation has proved to be a suitable synthesis technique in several applications ranging from sum and difference antennas [7] and phase switched screens [13] up to airborne pulse doppler radars [8]. As a matter of fact, the improved flexibility of the antenna design which allows to generate several patterns with different shapes [7] and sidelobe levels (SLL) [2] without the need of changing the static excitations as well as the possibility to synthesize patterns while keeping very low dynamic range ratios [11] represent non-negligible advantages of the time-modulation strategy. Some experimental prototypes have been also recently built and tested in [6][13]. Besides the numerical analyses and the experimental validations, a detailed mathematical description of the key antenna parameters in TM arrays (e.g., gain and directivity) has been also presented [2][14][15].

The main disadvantage of TM arrays is related to the *sideband radiations* (SBRs) due to the losses in the integer harmonics of the modulation frequency [15]. To avoid this drawback, different optimization algorithms aimed at minimizing the sideband levels (SBLs) (i.e., the peak levels of the harmonic radiations) have been used. Approaches based on the Differential Evolution (DE) [3], the Simulated Annealing (SA) [5], and the Genetic Algorithm (GA) [6] have been successfully applied. A different strategy exploiting time sequences with arbitrary *switch-on* instants has been also presented in [16]. However, due to the heavy computational burden for the computation of the harmonic patterns and the successive evaluation of the SBLs, the optimization has been usually limited to the first harmonic terms [3][4][5]. Recently, a simple closed-form relationship of the total power associated to the SBRs, derived in [15] for TM linear arrays, has enabled an easy and complete computation of the power losses.

This paper is then aimed at firstly extending the mathematical formulation in [15] to planar arrays where the losses at the harmonic frequencies are even more relevant due to the larger

number of elements usually involved. Successively, an optimization procedure based on a Particle Swarm Optimizer (PSO) [17] is used to fully exploit the analytic expression of the SBRs for minimizing the power losses.

The outline of the paper is as follows. The radiation of time-modulated planar arrays ($TMPA$) is mathematically described in Sect. 2 where a closed-form relationship for the SBRs is determined and minimized by means of a PSO. In Sect. 3, a selected set of results from an extensive set of numerical simulations is reported and discussed. Eventually, some conclusions are drawn (Sect. 4).

2 Mathematical Formulation

Let us consider a planar array with $M \times N$ elements displaced on a regular grid along the $x-y$ plane. The *static* set of element excitations $\underline{A} = \{\alpha_{mn};\, m = 0, ..., M-1,\, n = 0, ..., N-1\}$ is modulated by means of periodic rectangular pulse functions generated by RF switches inserted into the antenna feed network to obtain *dynamic* excitations. The array factor is then given by

$$AF(\theta, \phi, t) = e^{j\omega_0 t} \sum_{m=0}^{M-1} \sum_{n=0}^{N-1} \alpha_{mn} g_{mn}(t)\, e^{j\beta \sin\theta (x_m \cos\phi + y_n \sin\phi)} \tag{1}$$

where $x_m = m \times d_x$ and $y_n = n \times d_y$ denote the location of the mn-th array element, $\beta = \frac{\omega_0}{c}$ is the free-space wave number, ω_0 and c being the carrier angular frequency and the speed of light in vacuum, respectively. Moreover, the time behavior of the RF switches is mathematically modeled through the function $g_{mn}(t) = g_{mn}(t + iT_p)$, i and T_p being an integer value and the modulation period, respectively. As for the linear case, such a periodic function can be expressed in terms of its Fourier coefficients

$$g_{mn}(t) = \sum_{h=-\infty}^{\infty} G_{mnh} e^{jh\omega_p t},\ m = 0, ..., M-1,\, n = 0, ..., N-1 \tag{2}$$

where $\omega_p = \frac{2\pi}{T_p}$ and G_{mnh} is a real quantity if $g_{mn}(t)$ is considered to be

$$g_{mn}(t) = \begin{cases} 1 & if\ \ 0 < |t| \leq \frac{\widetilde{t}_{mn}}{2} \\ 0 & otherwise \end{cases} \tag{3}$$

equal to

$$G_{mnh} = \frac{1}{T_p} \int_{-T_p/2}^{T_p/2} g_{mn}(t) e^{-jh\omega_p t} dt. \tag{4}$$

Thanks to this expansion, the array factor (1) results a summation of infinite harmonics [15], $AF(\theta, \phi, t) = \sum_{h=-\infty}^{\infty} AF_h(\theta, \phi, t)$, where

$$AF_0(\theta, \phi) = \sum_{m=0}^{M-1} \sum_{n=0}^{N-1} \alpha_{mn} \tau_{mn} e^{j\beta \sin\theta (x_m \cos\phi + y_n \sin\phi)} \tag{5}$$

is the pattern at the working frequency ($h = 0$), being $\tau_{mn} = \frac{\widetilde{t}_{mn}}{T_p} = G_{mn0}$, and the h-th harmonic term is given by

$$AF_h(\theta, \phi, t) = e^{j(\omega + h\omega_p)t} \sum_{m=0}^{M-1} \sum_{n=0}^{N-1} \alpha_{mn} G_{mnh} e^{j\beta \sin\theta (x_m \cos\phi + y_n \sin\phi)}. \tag{6}$$

The power radiated by a $TMPA$ defined as

$$\mathcal{P}_{TOT} = \frac{1}{T_p} \int_{-T_p/2}^{T_p/2} \left[\int_0^{2\pi} \int_0^{\pi} Re\left\{ AF(\theta, \phi, t) \right\}^2 sin\theta d\theta d\phi \right] dt \tag{7}$$

turns out to be equal to

$$\mathcal{P}_{TOT} = \int_0^{2\pi} \int_0^{\pi} \frac{1}{2} \sum_{h=-\infty}^{\infty} \left| \mu_h(\theta, \phi) \right|^2 sin\theta d\theta d\phi \tag{8}$$

where $\mu_h(\theta, \phi) = \sum_{m=0}^{M-1} \sum_{n=0}^{N-1} \alpha_{mn} G_{mnh} e^{j\beta \sin\theta (x_m \cos\phi + y_n \sin\phi)}$, while the power losses associated to the sideband radiations are given by

$$\mathcal{P}_{SBR} = \frac{1}{2} \int_0^{2\pi} \int_0^{\pi} \sum_{h=-\infty, h\neq 0}^{\infty} \left| \mu_h(\theta, \phi) \right|^2 sin\theta d\theta d\phi. \tag{9}$$

Since $\left| \mu_h(\theta, \phi) \right|^2 = \mu_h(\theta, \phi) \left[\mu_h(\theta, \phi) \right]^*$ and taking into account the following relationship from [15]

$$\sum_{h=-\infty, h\neq 0}^{\infty} G_{mnh} G_{rsh} = \Delta\tau_{mn}^{rs} - \tau_{mn}\tau_{rs} \tag{10}$$

where $\Delta\tau_{mn}^{rs} = \tau_{mn}$ if $\tau_{mn} \leq \tau_{rs}$ and $\Delta\tau_{mn}^{rs} = \tau_{rs}$ otherwise, Equation (9) can be rewritten as follows

$$\mathcal{P}_{SBR} = 2\pi \sum_{m=0}^{M-1} \sum_{n=0}^{N-1} \sum_{r=0}^{M-1} \sum_{s=0}^{N-1} \left[Re\left\{ \alpha_{mn} \alpha_{rs}^* \right\} \frac{sin\left(\beta \sqrt{(x_m - x_r)^2 + (y_n - y_s)^2} \right)}{\beta \sqrt{(x_m - x_r)^2 + (y_n - y_s)^2}} \left(\Delta\tau_{mn,rs} - \tau_{mn}\tau_{rs} \right) \right] \tag{11}$$

after simple manipulations detailed in **Appendix**.

For square ($N \times N$) planar arrays, Equation (11) simplifies

$$\mathcal{P}_{SBR} = 2\pi \sum_{m,\,n=0}^{N-1} \left[|\alpha_{mn}|^2 \tau_{mn}(1-\tau_{mn}) \right] + \\ +2\pi \sum_{m,\,n=0,\,(r,s)\neq(m,n)}^{N-1} \left[Re\left\{\alpha_{mn}\alpha_{rs}^*\right\} \frac{sin\left(\beta\sqrt{(x_m-x_r)^2+(y_n-y_s)^2}\right)}{\beta\sqrt{(x_m-x_r)^2+(y_n-y_s)^2}} \left(\Delta\tau_{mn}^{rs} - \tau_{mn}\tau_{rs}\right) \right]. \tag{12}$$

2.1 PSO-based Power Losses Minimization

The analytic form of $\mathcal{P}_{SBR}$ [Eq. (11)] enables a computationally-efficient optimization of the power losses in $TMPA$s. Towards this end, the problem unknowns are the *static* excitation coefficients, $\underline{A} = \{\alpha_{mn};\, m = 0, ..., M-1,\, n = 0, ..., N-1\}$, and the set of *switch-on times*, $\underline{\tau} = \{\tau_{mn};\, m = 0, ..., M-1,\, n = 0, ..., N-1\}$. Let us assume a fixed set of *static* excitations, $\underline{A} = \hat{\underline{A}}$. Therefore, the use of time-pulses would allow an initial pattern (generated by the static excitation distribution) to be reconfigured by the insertion of the on-off switches between the generator and the array elements, avoiding a new feeding network design that would be necessary if time-modulation were not applied.

The minimization of the losses is then recast as the solution of an equivalent optimization problem mathematically formulated in terms of the following cost function

$$\Psi\left\{\underline{\tau}_k\right\} = w_{SLL} H\left[\widetilde{SLL} - SLL\left(\underline{\tau}_k\right)\right] \frac{\left|\widetilde{SLL} - SLL\left(\underline{\tau}_k\right)\right|^2}{\left|\widetilde{SLL}\right|^2} + w_{SBR} \frac{\mathcal{P}_{SBR}\left(\underline{\tau}_k\right)}{\mathcal{P}_{TOT}\left(\underline{\tau}_k\right)} \tag{13}$$

and aimed at defining the optimal set $\underline{\tau}_{opt}$ at the convergence of an iterative process, k being the iteration index. Moreover, $H(\cdot)$ is the Heaviside step function, while w_{SLL} and w_{SBR} are real and positive weights. The first term in (13), Ψ_{SLL}, penalizes quantifies the mismatch between the sidelobe level generated at $h = 0$ by $\underline{\tau}_k$, $SLL\left(\underline{\tau}_k\right)$, and the desired one, $\widetilde{SLL}$, whether $SLL\left(\underline{\tau}_k\right) > \widetilde{SLL}$. It acts like a constraint of the minimization of the power losses forced by the other term, Ψ_{SBR}.

Since the unknown set $\underline{\tau}_k$ is real-valued, the minimization of (13) is carried out by means of a Particle Swarm Optimizer (PSO) [17] whose implementation is detailed in [18]. The iterative process stops when a maximum number of iterations K is reached or at the stationariness of

the value of $\Psi_k^{opt} = \Psi\left\{\underline{\tau}_k^{opt}\right\}$, $\underline{\tau}_k^{opt} = arg\left\{min_{s=1,\dots,S}\left[\Psi\left(\underline{\tau}_k^{(s)}\right)\right]\right\}$, S being the number of particles/agents of the swarm.

3 Numerical Results

A set of representative results is here reported to show the potentialities of the proposed method for the synthesis of $TMPA$ with reduced SBRs. The first example deals with a planar array having circular contour, while the second one is concerned with the synthesis of a rectangular arrangement. As regards the PSO, the control parameters have been set to the values derived in [18], namely $\omega = 0.4$ (inertial weight), $C_1 = 2.0$ (cognitive acceleration coefficient), $C_2 = 2.0$ (social acceleration coefficient).

In the first example, the array elements are placed on a regular grid of dimension $N \times M = 20 \times 20$ with inter-elements spacing equal to $d_x = d_y = 0.5\lambda$ and the antenna contour has radius $r = 5\lambda$, $\lambda = cT_0$ being the free space wavelength. Thus, the number of radiating array elements amounts to $L = 316$, while the other 84 elements laying outside the circular contour are deleted from the grid (i.e., $\alpha_{mn} = 0$). Starting from a set of *static* excitation $\underline{\hat{A}}$ obtained through the sampling of the Taylor distribution ($SLL = -30\,dB$, $\bar{n} = 6$ [19]) and affording a pattern with $SLL = -29.25\,dB$ [20] and because of the quadrantal symmetry of the array architecture, a quarter of the total number of elements, $U = 79$, has been optimized for the synthesis of a broadside pencil beam pattern. The cost function (13) has been then minimized with a swarm of $S = 30$ particles. The value $\widetilde{SLL}$ has been set to $-40\,dB$ and the weight coefficients have been heuristically tuned to $w_{SLL} = 2$ and $w_{SBR} = 1$. Moreover, $K = 2000$ iterations have been considered and, at the initialization, the *switch-on times* have been randomly-generated with uniform probability within $\tau_{mn}^{(0)} \in [0, 1]$, $\forall(m, n)$.

The normalized power pattern generated at the central frequency is shown in Fig. 1. The level of the secondary lobes is reduced of almost $8\,dB$ ($SLL_{opt} = -37.8\,dB$) compared to that afforded with the *static* excitations and the power wasted in SBRs amounts to $\mathcal{P}_{SBR} = 13.2\%$ of the total input power. The PSO-optimized pulse sequence $\underline{\tau}_{opt}$ is reported in Fig. 2(*a*) together with the distribution of the static excitations [Fig. 2(*b*)].

For completeness, the behavior of the cost function Ψ_k^{opt} along the iterative optimization process

is shown in Fig. 3, while the patterns at the first ($|h| = 1$) and the second ($|h| = 2$) harmonics are shown in Fig. 4(*a*) and Fig. 4(*b*), respectively.

The second test deals with a square array with $N \times M = 10 \times 10$ elements located on the same grid of the previous example. In this case, the *static* element excitations are uniformly-distributed: $\alpha_{mn} = 1$, $\forall(m, n)$. The array factor at $h = 0$ can be expressed either through (5) or, assuming the *separable distribution* condition for the dynamic excitations, as the product of the array factors of two linear arrays of M and N elements along the x and y axes, respectively

$$AF_0(\theta, \phi) = \sum_{m=0}^{M-1} \alpha_m \tau_m e^{j\beta x_m sin\theta cos\phi} \sum_{n=0}^{N-1} \alpha_n \tau_n e^{j\beta y_n sin\theta sin\phi}. \quad (14)$$

Moreover, the following relationships hold true

$$\alpha_m \tau_m = \frac{\alpha_{m0}\tau_{m0}}{\alpha_{00}\tau_{00}} \ , \ \alpha_n \tau_n = \frac{\alpha_{0n}\tau_{0n}}{\alpha_{00}\tau_{00}} \quad (15)$$

$m = 0, ..., M-1$ and $n = 0, ..., N-1$.

The number of unknowns in the non-separable case [Eq. (5)] is equal to $U = 25$ (i.e., a quarter of the total number of elements $L = 100$), while the separable case [Eq. (14)] considers only $U = 10$ variables. As regards the optimization, a swarm of $S = 15$ particles has been used with a maximum number of iterations equal to $K = 1000$. Moreover, the constraint on the sideband level has been set to $\widetilde{SLL} = -20\,dB$.

At the end of the PSO-based optimization, the patterns in Fig. 5(*a*) and Fig. 5(*b*) have been synthesized for the non-separable case (NSD) and the separable one (SD), respectively. The level of the sidelobes is equal to $SLL_{NSD} = -19.6\,dB$ and $SLL_{SD} = -19.4\,dB$, respectively. Moreover, the secondary lobes behave differently (Fig. 5). As expected, higher levels verify along the orthogonal axis of the array (i.e., the x and y axes) in correspondence with the separable distribution [Fig. 5(*b*)]. On the contrary, the energy wasted outside the main lobe is more uniformly-distributed within the visible range in Fig. 5(*a*).

The optimized time-sequences are shown in Fig. 6. More in detail, Figure 6(*a*) shows that 9 among 25 elements are switched-off, while the *switch-on times* of the separable distribution [Fig. 6(*b*)] satisfy (15).

Thanks to the larger number of degrees of freedom ($U_{NSD} = 25$ vs. $U_{SD} = 9$), the power losses

in the SBRs result lower than 3% (i.e., $\mathcal{P}_{SBR} = 2.8\%$), while they rise to $\mathcal{P}_{SBR} = 11.1\%$ for the pattern synthesized with the optimized separable distribution. The non-negligible reduction of $\mathcal{P}_{SBR}$ has also a positive effect on the SBLs of the harmonic radiations. Figure 7 shows the patterns generated by the pulse sequence in Figs. 6(*a*)-6(*b*) at the first ($|h| = 1$) [Figs. 7(*a*)-(*b*)] and the second ($|h| = 2$) [Figs. 7(*c*)-(*d*)] harmonic terms. The SBLs of the patterns generated optimizing $U_{NSD} = 25$ elements [Figs. 7(*a*)-(*c*)] are much lower than those obtained when $U_{SD} = 10$ [Figs. 7(*b*)-(*d*)]. More specifically, $SBL^{(1)}_{NSD} = -31.8\,dB$ vs. $SLL^{(2)}_{SD} = -20.2\,dB$ and $SBL^{(1)}_{NSD} = -33.1\,dB$ vs. $SLL^{(2)}_{SD} = -22.9\,dB$. For completeness, the values of the SBLs until $h = 20$ are reported in Fig. 8.

As far as the iterative minimization is concerned, the convergence has been yielded in the separable case only after 226 iterations, while the maximum number of iterations ($K = 1000$) have been necessary otherwise to get the final solution because of the wider solution space to be sampled during the optimization.

4 Conclusions

In this paper, the minimization of the power losses in time-modulated planar arrays has been carried out by means of an effective PSO-based optimization strategy thanks to the definition of an analytical closed-form relationship that allows a simple and complete computation of the power losses in the infinite sideband radiation patterns. The obtained results have shown the effectiveness of the proposed method as a reliable alternative to other approaches aimed at optimizing the SBLs at the first harmonic terms. The use of either separable and non-separable coefficient distributions has been also analyzed to point out that the sideband radiations can be effectively reduced exploiting a larger number of degrees of freedom, but at the cost of an increased computational burden.

Appendix

The solution of the integral in Eq. (9) is here derived.

The integral can be rewritten as

$$I = \int_0^{\pi} I_\theta sin\theta d\theta \tag{16}$$

where

$$I_\theta = \int_{-\pi}^{\pi} e^{j(acos\phi + bsin\phi)} d\phi \tag{17}$$

being $a = \beta sin\theta(x_m - x_r)$ and $b = \beta sin\theta(y_n - y_s)$. By considering the Euler relationships

$$acos\phi + bsin\phi = a\frac{\left(e^{j\phi} + e^{-j\phi}\right)}{2} + b\frac{\left(e^{j\phi} - e^{-j\phi}\right)}{2j} = \sqrt{a^2 + b^2} sin\left[\phi + atan\left(\frac{a}{b}\right)\right] \tag{18}$$

and after simple mathematical manipulations, it can be proved that

$$I_\theta = \int_{-\pi}^{\pi} e^{j\sqrt{a^2+b^2}\sin\left[\phi + atan\left(\frac{a}{b}\right)\right]} d\phi \tag{19}$$

whose closed-form solution in terms of Bessel functions turns out to be [21]

$$I_\theta = 2\pi J_0(\sqrt{a^2 + b^2}). \tag{20}$$

Therefore, Equation (16) reduces to

$$I = 2\pi \int_0^{\pi} J_0(\sqrt{a^2 + b^2})\sin\theta d\theta \tag{21}$$

or in its explicit form [22]

$$I = 4\pi \frac{sin\left(\beta\sqrt{(x_m - x_r)^2 + (y_n - y_s)^2}\right)}{\left(\beta\sqrt{(x_m - x_r)^2 + (y_n - y_s)^2}\right)}. \tag{22}$$

References

[1] Shanks, H. E., and Bickmore, R. W.: 'Four-dimensional electromagnetic radiators', *Canad. J. Phys.*, 1959, 37, pp. 263-275.

[2] Kummer, W. H., Villeneuve, A. T., Fong, T. S., and Terrio, F. G.: 'Ultra-low sidelobes from time-modulated arrays', *IEEE Trans. Antennas Propag.*, 1963, 11, (6), pp. 633-639.

[3] Yang, S., Gan, Y. B., and Qing, A.: 'Sideband suppression in time-modulated linear arrays by the differential evolution algorithm', *IEEE Antennas Wireless Propag. Lett.*, 2002, 1, pp. 173-175.

[4] Yang, S., Gan, Y. B., and Tan, P. K.: 'A new technique for power-pattern synthesis in time-modulated linear arrays', *IEEE Antennas Wireless Propag. Lett.*, 2003, 2, pp. 285-287.

[5] Fondevila, J., Brégains, J. C., Ares, F., and Moreno, E.: 'Optimizing uniformly excited linear arrays through time modulation', *IEEE Antennas Wireless Propag. Lett.*, 2004, 3, pp. 298-301.

[6] Yang, S., Gan, Y. B., Qing, A., and Tan, P. K.: 'Design of a uniform amplitude time modulated linear array with optimized time sequences', *IEEE Trans. Antennas Propag.*, 2005, 53, (7), pp. 2337-2339.

[7] Fondevila, J., Brégains, J. C., Ares, F., and Moreno, E.: 'Application of time modulation in the synthesis of sum and difference patterns by using linear arrays', *Microw. Opt. Technol. Lett.*, 2006, 48, (5), pp. 829-832.

[8] Li, G., Yang, S., and Nie, Z.: 'A study on the application of time modulated antenna arrays to airborne pulsed doppler radar', *IEEE Trans. Antennas Propag.*, 2009, 57, (5), pp. 1578-1582.

[9] Yang, S., Nie, Z., and Yang, F.: 'Synthesis of low sidelobe planar antenna arrays with time modulation'. *Proc. APMC 2005 Asia-Pacific Microw. Conf.*, Suzhou, China, Dec. 2005, p. 3.

[10] Yang, S., and Nie, Z.: 'Time modulated planar arrays with square lattices and circular boundaries', *Int. J. Numer. Model.*, 2005, 18, pp. 469-480.

[11] Chen, Y., Yang, S., and Nie, Z.: 'Synthesis of satellite footprint patterns from time-modulated planar arrays with very low dynamic range ratios', *Int. J. Numer. Model.*, 2008, 21, pp. 493-506.

[12] Chen, Y., Yang, S., and Nie, Z.: 'Synthesis of optimal sum and difference patterns from time-modulated hexagonal planar arrays', *Int. J. Infrared Milli. Waves*, 2008, 29, pp. 933-945.

[13] Tennant, A., and Chambers, B.: 'Time-switched array analysis of phase-switched screens', *IEEE Trans. Antennas Propag.*, 2009, 57, (3), pp. 808-812.

[14] Yang, S., Gan, Y. B., and Tan, P. K.: 'Evaluation of directivity and gain for time-modulated linear antenna arrays', *Microw. Opt. Technol. Lett.*, 2004, 42, (2), pp. 167-171.

[15] Brégains, J. C., Fondevila, J., Franceschetti, G., and Ares, F.: 'Signal radiation and power losses of time-modulated arrays', *IEEE Trans. Antennas Propag.*, 2008, 56, (6), pp. 1799-1804.

[16] Tennant, A., and Chambers, B.: 'Control of the harmonic radiation patterns of time-modulated antenna arrays'. *Proc. 2008 IEEE AP-S International Symp.*, S. Diego, CA (USA), July 2008.

[17] Kennedy, J., Eberhart, R. C., and Shi, Y.: '*Swarm Intelligence*' (Morgan Kaufmann, 2001).

[18] Donelli, M., and Massa, A.: 'Computational approach based on a particle swarm optimizer for microwave imaging of two-dimensional dielectric scatterers', *IEEE Trans. Microw. Theory Tech.*, 2005, 53, (5), pp. 1761-1776.

[19] Taylor, T. T.: 'Design of a circular aperture for narrow beamwidth and low sidelobes', *IRE Trans. Antennas Propag.*, 1960, 8, pp. 17-22.

[20] Elliott, R. S. : *'Antenna Theory and Design*' (Wiley, 2003).

[21] Gradshteyn, I. S., and Ryzhik, I. M.: *'Table of Integrals, Series, and Products'*. (Academic Press, 2000).

[22] Rudge, A. W., Milne, K., Oliver, A. D., and Knight, P.: *'The handbook of antenna design*'. (IEE Electromagnetic Waves Series, 1986).

FIGURE CAPTIONS

- **Figure 1.** *Circular Aperture* ($N = M = 20$, $L = 316$, Taylor [19] $SLL = -30\,dB$, $\bar{n} = 6$) - Normalized power pattern at the carrier frequency ($h = 0$).

- **Figure 2.** *Circular Aperture* ($N = M = 20$, $L = 316$, Taylor [19] $SLL = -30\,dB$, $\bar{n} = 6$) - Distribution of (*a*) the optimized switch-on times $\underline{\tau}_{opt}$ and (*b*) the static element excitations.

- **Figure 3.** *Circular Aperture* ($N = M = 20$, $L = 316$, Taylor [19] $SLL = -30\,dB$, $\bar{n} = 6$) - Behavior of the cost function terms during the iterative PSO-based optimization.

- **Figure 4.** *Circular Aperture* ($N = M = 20$, $L = 316$, Taylor [19] $SLL = -30\,dB$, $\bar{n} = 6$) - Normalized power patterns at (*a*) the first ($h = 1$) and (*b*) the second ($h = 2$) harmonics.

- **Figure 5.** *Rectangular Aperture* ($N = M = 10$, $L = 100$, $\alpha_{mn} = 1$) - Normalized power patterns at the carrier frequency ($h = 0$) for (*a*) the non-separable case and (*b*) the separable one.

- **Figure 6.** *Rectangular Aperture* ($N = M = 10$, $L = 100$, $\alpha_{mn} = 1$) - Distribution of the optimized switch-on times $\underline{\tau}_{opt}$ for (*a*) the non-separable and (*b*) the separable cases.

- **Figure 7.** *Rectangular Aperture* ($N = M = 10$, $L = 100$, $\alpha_{mn} = 1$) - Normalized power patterns at (*a*)(*b*) the first ($|h| = 1$) and (*c*)(*d*) the second ($|h| = 2$) terms in correspondence with (*a*)(*c*) the NSD case and (*b*)(*d*) the SD one.

- **Figure 8.** *Rectangular Aperture* ($N = M = 10$, $L = 100$, $\alpha_{mn} = 1$) - Behavior of the sideband levels, $SBL^{(h)}$, $h \in [0,\, 20]$, of the solutions synthesized in the NSD and the SD cases.

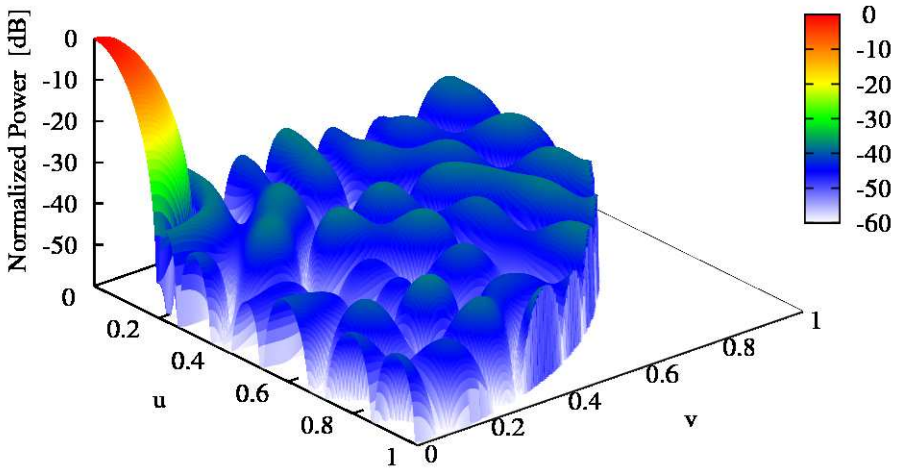

Fig. 1 - L. Poli *et al.,* “Analysis and Optimization of the Sideband Radiations ...”

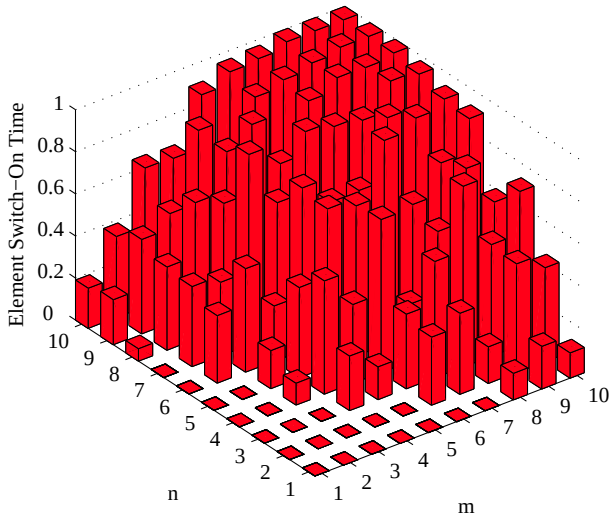

(a)

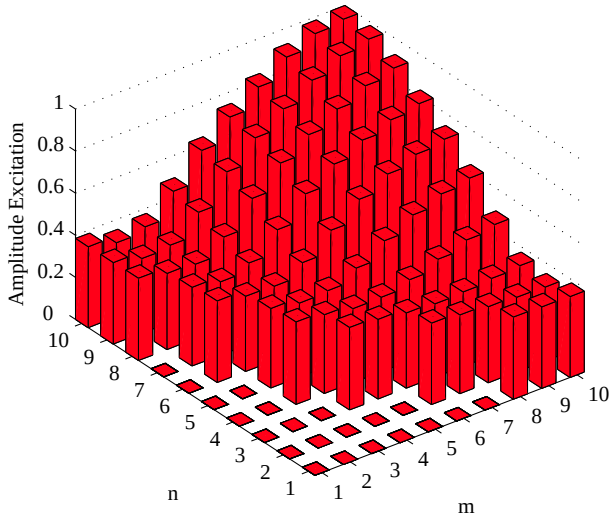

(b)

Fig. 2 - L. Poli *et al.,* "Analysis and Optimization of the Sideband Radiations ..."

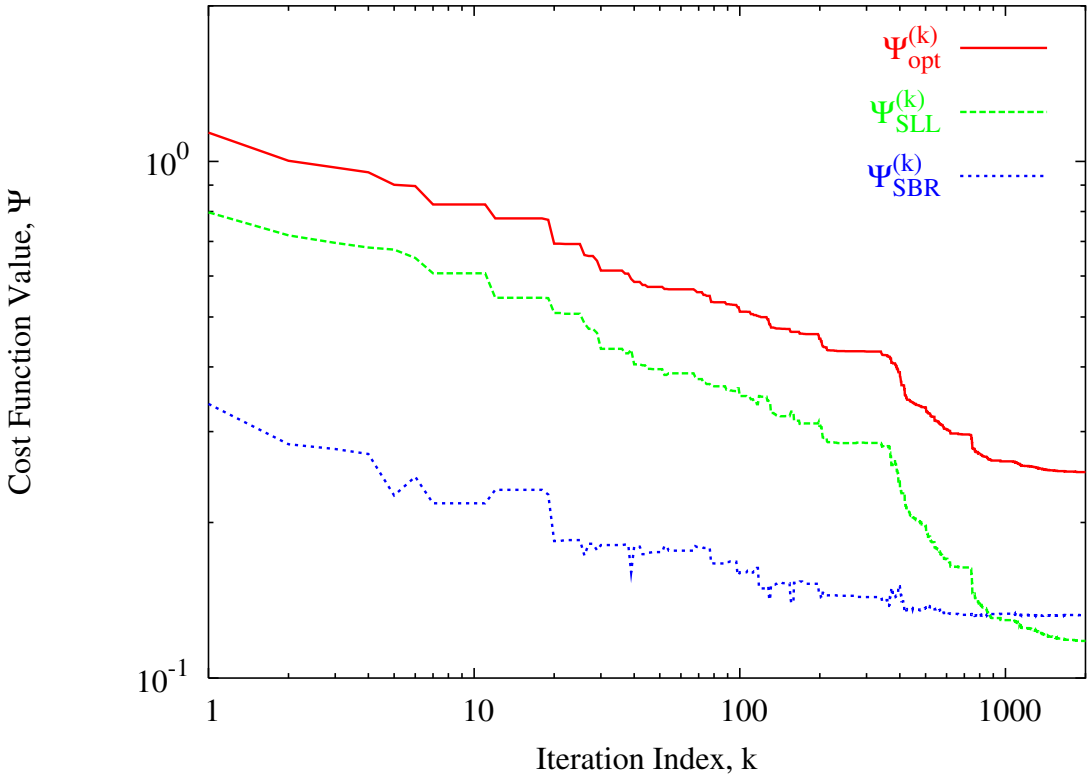

Fig. 3 - L. Poli *et al.,* "Analysis and Optimization of the Sideband Radiations ..."

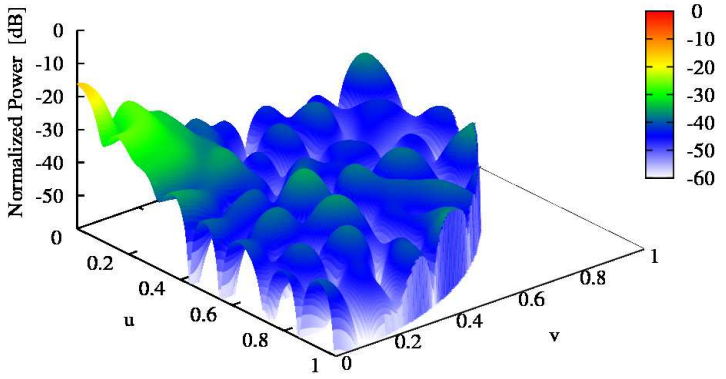

(a)

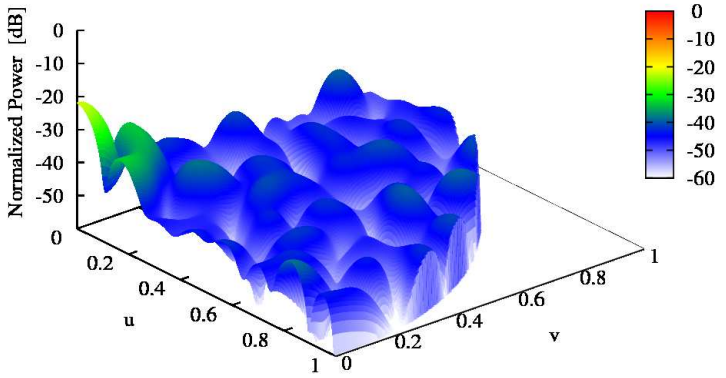

(b)

Fig. 4 - L. Poli *et al.*, "Analysis and Optimization of the Sideband Radiations ..."

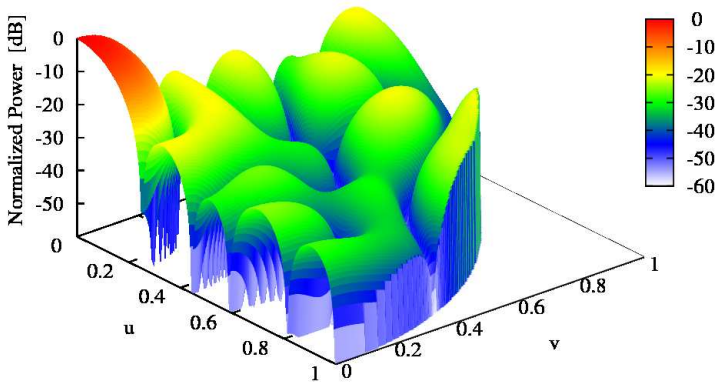

(a)

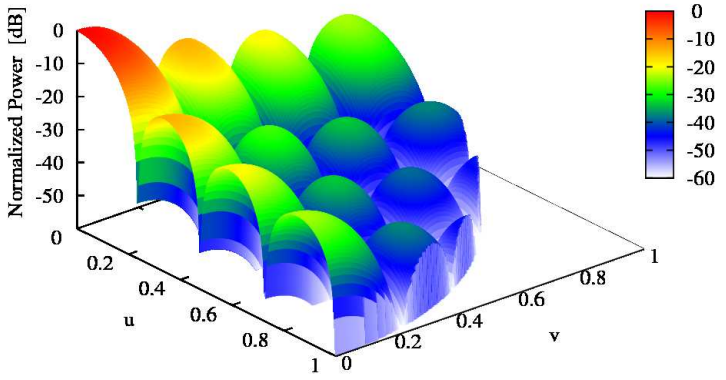

(b)

Fig. 5 - L. Poli *et al.*, "Analysis and Optimization of the Sideband Radiations ..."

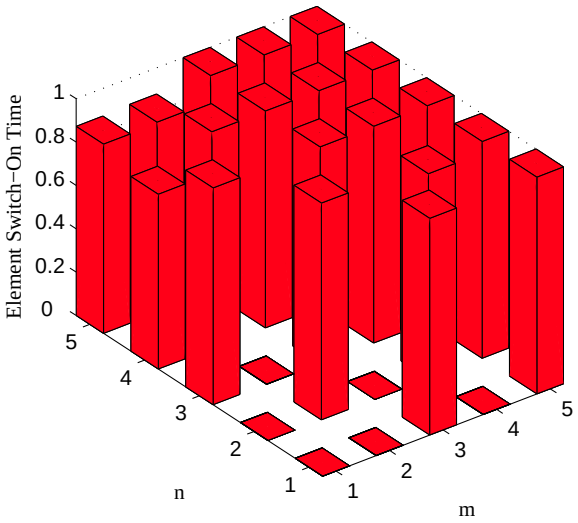

(a)

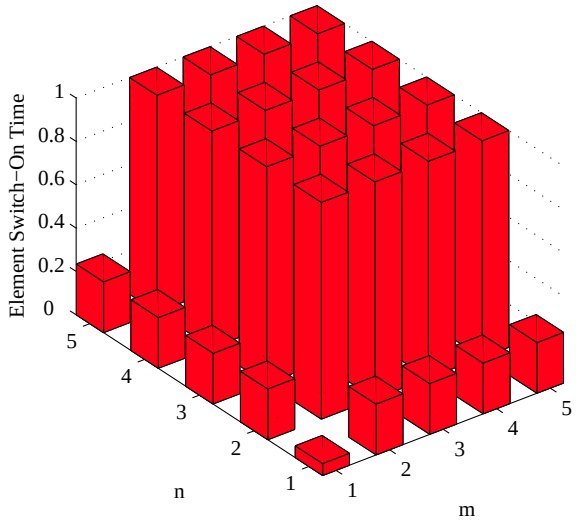

(b)

Fig. 6 - L. Poli *et al.,* “Analysis and Optimization of the Sideband Radiations ...”

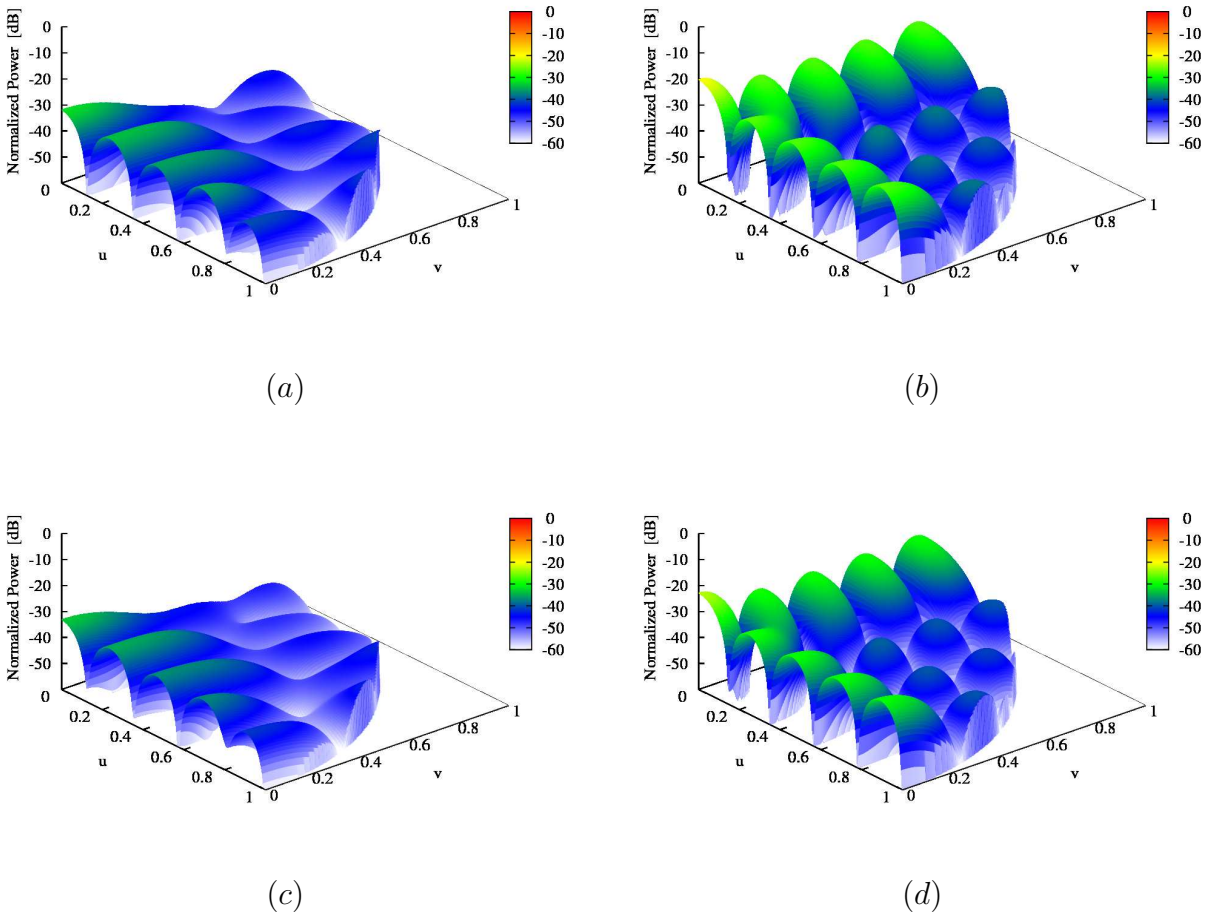

Fig. 7 - L. Poli *et al.*, "Analysis and Optimization of the Sideband Radiations ..."

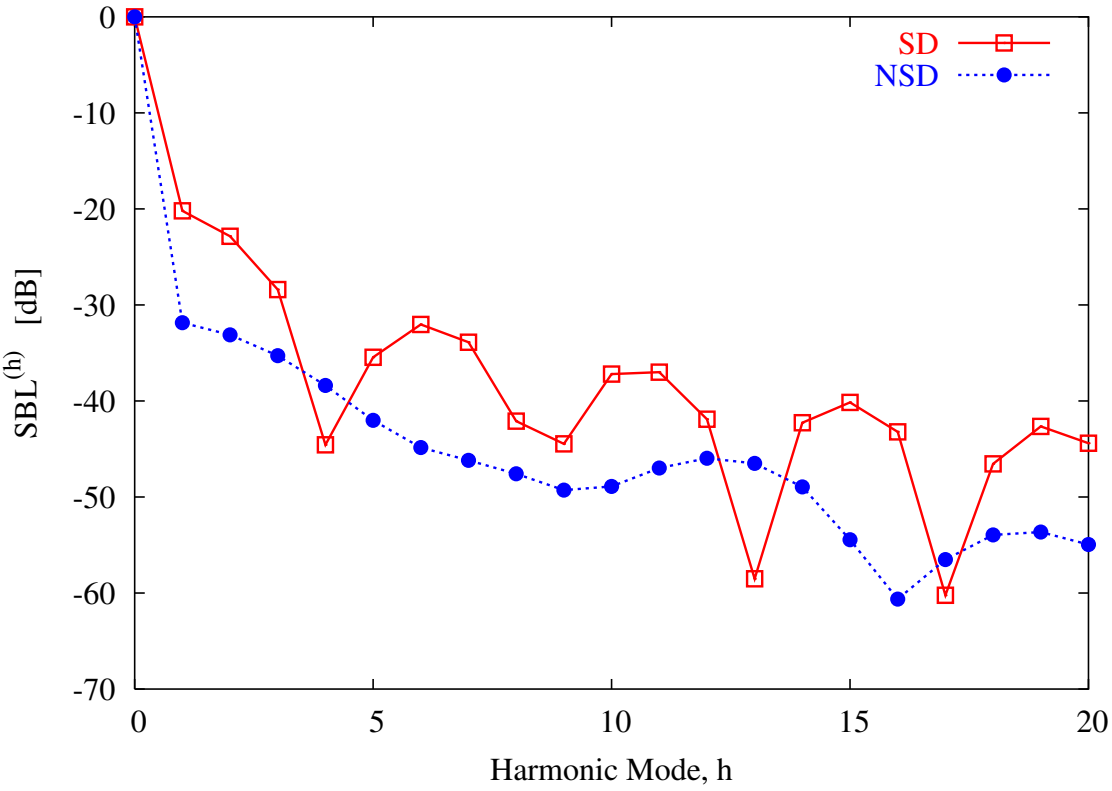

Fig. 8 - L. Poli *et al.,* "Analysis and Optimization of the Sideband Radiations ..."